Received: Added at production | Revised: Added at production | Accepted: Added at production

DOI: xxx/xxxx

ARTICLE TYPE

Speed-Current Single-loop Control of PMSM Based on Model-Assisted Cascaded Extended State Observer and Sliding Mode Control

Min Wang[1] | Yanhong Liu[1] | Qi Wang[1] | Yuefeng Liao*[1] | Patrick Wheeler[2]

[1]the School of Electrical and Information Engineering, Zhengzhou University, Zhengzhou 450001, China.
[2]the Power Electronics, Machines and Control Group, University of Nottingham, Nottingham NG7 2RD, U.K.

Correspondence
*Yuefeng Liao, the School of Electrical and Information Engineering, Zhengzhou University, Zhengzhou 450001, China.
Email: liaoyuefeng@zzu.edu.cn

Summary

This paper proposes a novel speed-current single-loop speed regulation controller for PMSM based on model-assisted cascaded extended state observer (ESO) and sliding mode control (SMC), aimed at simplifying the control structure, increasing dynamic performance and improving anti-disturbance performance. Firstly, a cascaded ESO based on model information is designed for the second-order model of single-loop control of PMSM. This approach allows for quick and accurate estimation of disturbance without increasing bandwidth, while also reducing the burden of ESO with model-assisted information. Next, with the estimation disturbance feedforward compensation, the composite controller is constructed based on SMC, which effectively eliminates residual disturbance and reduces chatterings. The stability of the closed-loop system under the proposed controller is proved strictly. Finally, simulations and experiments are conducted to validate the effectiveness and robustness of the proposed method.

KEYWORDS:
PMSM, speed-current single-loop control, speed regulation, model-assisted cascaded ESO, SMC

1 | INTRODUCTION

Permanent Magnet Synchronous Motor (PMSM) is widely used in high-performance servo systems and various industrial applications due to its high efficiency and power density[1–3]. However, achieving high tracking accuracy, strong robustness and excellent security remains a central challenge in PMSM drive system design. In the control of PMSM system, many control methods have been applied, such as PI control[4], fuzzy control[5], neural network control[6], model predictive control[7–8], active disturbance rejection control(ADRC)[9] and SMC[10]. The PI control method is usually adopted in the speed and current control of PMSM[4]. However, there is a conflict between system stability and dynamic performance because PI controller is linear. The construction of membership function of fuzzy control needs manual experience, which is difficult to obtain[5]. Because of the complexity of computation, the application of neural network to PMSM requires high-quality hardware[6]. Model predictive control does not need to adjust the parameters, but reduces the control effect if there is parameter variation[11].

ADRC and SMC are considered to be effective methods for improving the capacity of resisting disturbance and robustness of PMSM systems and other practical systems[12–15]. Conventional ADRC is a combination of PD control and the feedforward of ESO. In the ADRC scheme, the key element is the ESO[16], which is responsible for estimating unmeasurable state variables and lumped disturbance[17]. Furthermore, the states estimated with ESO have less chatterings and are better than those measured with

hardware. However, the PD controller in ADRC is linear, which limits the control effect of ADRC to some extend. Although the SMC achieves good robustness, due to the existence of sign function, there is the phenomenon of chatterings, which would be critical in PMSM systems because of the upper bound of disturbance is relatively high [10].

Therefore, in order to further improve the robustness, the composite controller based on ESO and SMC have been proposed in PMSM. A composite method based on continuous fast terminal SMC and ESO was proposed in [18] and the disturbance estimated by ESO was compensated forward to reduce the chatterings of SMC. A speed regulation controller based on PI-SMC and ESO was developed in [19]. Based on PI-SMC with a new sliding-mode reaching law and ESO, Wang et al. constructed a speed regulation controller in [20]. A discrete compound controller of integral terminal SMC and ESO was proposed in [21]. With such above composite controllers, the required switching gain only needs to be greater than the upper bound of the disturbance estimation error, greatly reducing chattering of SMC. Additionally, SMC can eliminate residual disturbance and improve robustness.

However, the above composite methods based on ESO and SMC are all based on the double-loop structure of PMSM. As technology has advanced, there is little difference between the control period of the inner and outer loops of PMSM [22−23]. As an alternative to double-loop control, the speed-current single-loop structure has been applied, offering straightforward control design, simple parameter adjustment and satisfying system dynamic performance [24−25]. Despite its advantages, the single-loop structure inevitably brings the problem of unmatched disturbance. Under the single-loop structure, disturbances in the current loop are unmatched and enter the system via a different channel from the control input. These disturbances are mainly caused by external load torques, unmodeled dynamics and parameter perturbations, which have a negative impact on system performance and stability [26]. It is difficult to eliminate their influence from the output, posing a significant challenge for PMSM drive system design [27]. Therefore, a robust control method is needed to resist matched and unmatched disturbance in single-loop structure. To the best knowledge of authors, there are few papers based on ESO and SMC in single-loop structure of PMSM. A composite controller of three order ESO and backstepping sliding mode was constructed in speed regulation of PMSM in single-loop structure [28]. In [29], an ESO was designed to estimate the current and lumped disturbance simultaneously; then, the output-feedback SMC method was proposed by introducing the estimations.

However, the above strategies in both double-loop and single-loop structure are all based on conventional ESO. The conventional high-gain ESO has accurate estimation, but amplifying noise and without model information will further increase the estimation burden. The theory of observers reveals the existence of a trade-off between accuracy/speed of state reconstruction and sensitivity to high-frequency noise [30]. Increasing the bandwidth of ESO allows for faster estimation, but it also amplifies noise and then reduces the control performance. It is necessary to design an ESO that can increase estimation accuracy without increasing the bandwidth. In recent years, cascaded ESO has been the subject of research, which is capable of fast and accurate signal reconstruction while avoiding over-amplification of measurement noise [31]. However, the transfer function from the total disturbance to disturbance estimation error of cascaded ESO in the frequency domain has not been analysed. What's more, cascaded ESO has not been applied in speed-current single-loop structure systems of PMSM with matched and unmatched disturbance. Additionally, in practical application system, some known information such as model parameter in conventional ESO is estimated as part of lumped disturbance. ESO with model-assisted information can reduce the estimation burden compared to conventional ESO [32−33]. For PMSM system, the nominal values of its parameters are generally owned, so ESO with model-assisted information is more suitable for application to further reduce the estimation burden.

Motivated by the above survey, in order to simplify the control structure and improve anti-disturbance performance, this paper presents a novel speed-current single-loop controller to PMSM based on model-assisted cascaded ESO and SMC. Specifically, a cascaded ESO with model-assisted information is introduced to quickly and accurately estimate lumped disturbance without the need to increase bandwidth. Using the estimation disturbance feedforward compensation, the paper constructs a composite speed regulation controller based on SMC to improve robustness.

Compared with the previous related works, the main contributions and novelties of the paper are as follows.

1) A model-assisted cascaded ESO is designed to estimate the matched disturbance and unmatched disturbance for the second-order model of single-loop control of PMSM. This innovative approach not only allows for quick and accurate estimation of lump disturbance without increasing bandwidth, but also reduces the burden of ESO with model-assisted information.

2) It is proved that the observation error of model-assisted cascade ESO is bounded. The transfer function of total disturbance to disturbance estimation error is analyzed in the frequency domain, which shows that model-assisted cascade ESO is faster and more accurate than conventional ESO.

3) With the estimation disturbance feedforward compensation, the speed regulation composite controller is constructed based on model-assited cascaded ESO and SMC in single-loop structure of PMSM, which simplifies the control structure, increases dynamic performance, reduces the chatterings, and improves anti-disturbance performance.

4) The stability of the closed loop system under the composite algorithm is proved strictly. The influence of each parameter of the algorithm is analyzed in detail. Simulation and experiment demonstrate the effectiveness and robustness of the algorithm.

The remaining parts of the paper are organized as follows. Section 2 presents the mathematical model of PMSM. In section 3, a novel single-loop composite controller based on model-assisted cascaded ESO and SMC is proposed to simplify the control structure and improve anti-disturbance performance. Section 4 presents the simulative and experimental results. Finally, the conclusions are drawn in section 5.

2 | MATHEMATICAL MODEL OF PMSM

Based on typical d-q synchronously rotating reference frame, the mathematical model of surface-mounted PMSM in time domain can be described as follows

$$\begin{cases} \dot{i}_d = \dfrac{1}{L}\left(-R_s i_d + n_p \omega L i_q + u_d\right), \\ \dot{i}_q = \dfrac{1}{L}\left(-R_s i_q - n_p \omega L i_d - n_p \omega \Phi + u_q\right), \\ \dot{\omega} = \dfrac{1}{J_m}\left(\tau_e - \tau_L - B\omega\right), \end{cases} \tag{1}$$

where L is stator inductance, i_d and i_q are d-q axis stator current, u_d and u_q are d-q axis stator voltage, respectively. R_s is the stator resistance, n_p is the number of pole pairs, ω is the mechanical angular velocity, Φ is the rotor flux, J_m is the inertia, τ_L is the load torque disturbance, $\tau_e = \dfrac{3}{2} n_p \Phi i_q$ is the electromagnetic torque, B is the viscous friction coefficient.

In order to obtain the maximum torque-to-current ratio, the reference of d-axis current i_d^* is set to 0. If the controller of the d-axis current loop works properly, $i_d \doteq i_d^* = 0$ is attained[24], t hen the system of (1) with uncertainties can be described as,

$$\begin{cases} \dot{i}_q = \dfrac{1}{L}\left(-R_s i_q - n_p \omega \Phi + u_q\right) + d_q, \\ \dot{\omega} = \dfrac{1}{J_m}\left(\dfrac{3}{2} n_p \Phi i_q - B\omega\right) + d_\omega, \end{cases} \tag{2}$$

where d_q is matched disturbance, including parameter perturbations, unmodeled dynamic and external disturbance. d_ω is unmatched disturbance, including unknown load torque, parameter perturbations, unmodeled dynamic and external disturbance. d_q and d_ω are expressed as follows,

$$\begin{cases} d_q = \dfrac{-\Delta R_s i_q - n_p \omega \Delta\Phi - \Delta L \dot{i}_q}{L} - n_p \omega i_d + w_q, \\ d_\omega = -\dfrac{\tau_L}{J_m} + \dfrac{\dfrac{3}{2} n_p \Delta\Phi i_q - \Delta B\omega - \Delta J_m \dot{\omega}}{J_m} + w_\omega, \end{cases} \tag{3}$$

where ΔR_s, ΔL, $\Delta\Phi$, ΔJ_m and ΔB are the perturbations of the parameters R_s, L, Φ, J_m and B respectively. In addition, the external disturbances w_q and w_ω act on the current loop and the speed loop, respectively.

Based on the speed-current single-loop structure, the control system combines the speed loop and the current loop into a loop, and the second-order speed equation is established as follows,

$$\ddot{\omega} = -\frac{B}{J_m}\dot{\omega} + \frac{3 n_p \Phi}{2 J_m}\dot{i}_q + \dot{d}_\omega. \tag{4}$$

Substituting (2) into (4), the motion equation of PMSM can be written in the following form,

$$\ddot{\omega} = M\dot{\omega} + N\omega + g_q u_q + d_0, \tag{5}$$

where $M = -\dfrac{BL + J_m R_s}{J_m L}$, $N = -\dfrac{2BR_s + 3n_p^2\Phi^2}{2J_m L}$, $g_q = \dfrac{3n_p\Phi}{2J_m L}$ and $d_0 = \dfrac{3n_p\Phi}{2J_m} d_q + \dfrac{R_s}{L} d_\omega + \dot{d}_\omega$ is the lumped disturbance. For PMSM system, the nominal values of its parameters are generally owned, so M, N and g_q are known.

Assumption 1. The derivative of lumped disturbance d_0 is bounded and define $\zeta_0 = \sup_{t>0} ||\dot{d}_0||$.

The control objective is to construct a speed regulation controller based on model-assisted cascaded ESO and SMC for system (5) when PMSM is disturbed by matched and unmatched disturbance.

3 | CONTROLLER DESIGN

In this section, the cascaded ESO with model-assisted information is first proposed to estimate the lumped disturbance. In addition, the model-assisted cascaded ESO is analyzed in the frequency domain. Then, with the estimation disturbance and the estimation state $\hat{\omega}$ feedforward, the composite controller is constructed based on SMC. What's more, the stability of the closed-loop system under the proposed controller is proved. The overall algorithm process is shown in Fig. 1.

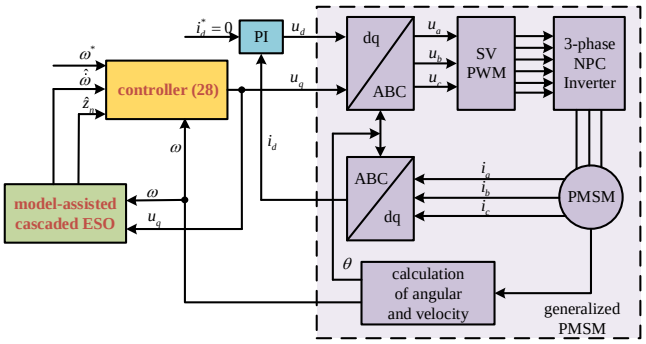

Figure 1 The overall algorithm process

3.1 | Model-Assisted Cascaded Extended State Observer

A cascaded ESO based on model information is designed below, which not only can estimate lump disturbance quickly without increasing bandwidth, but also can reduce the burden of ESO with model-assisted information. The model-assisted cascaded ESO is shown in Fig. 2.

Define $x_1 = \omega$, $x_2 = \dot{\omega}$, $x_3 = d_0$, then the system dynamic of (5) can be expressed as follows,

$$\begin{cases} \dot{x}_1 = x_2, \\ \dot{x}_2 = Mx_2 + Nx_1 + g_q u_q + x_3, \\ \dot{x}_3 = \dot{d}_0. \end{cases} \tag{6}$$

For the above equation, the first ESO with model-assisted information can be constructed to estimate state variables and lumped disturbance, designed as follows,

$$\begin{cases} \dot{z}_{11} = z_{12} + l_{11}\left(x_1 - z_{11}\right), \\ \dot{z}_{12} = Mz_{12} + Nz_{11} + g_q u_q + z_{13} + l_{12}\left(x_1 - z_{11}\right), \\ \dot{z}_{13} = l_{13}\left(x_1 - z_{11}\right), \end{cases} \tag{7}$$

where z_{11}, z_{12} and z_{13} are the estimations of x_1, x_2 and x_3. l_{11}, l_{12} and l_{13} are observer gains of the first ESO.

After the first ESO, the estimation error of disturbance is as

$$d_1 = x_3 - z_{13}. \tag{8}$$

Assumption 2. The derivative of d_1 is bounded and define $\zeta_1 = \sup_{t>0} ||\dot{d}_1||$.

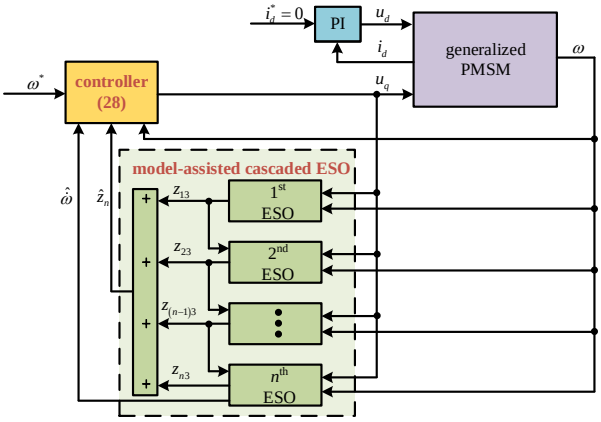

Figure 2 The model-assisted cascaded ESO

The second ESO model-assisted information is designed to estimate the state variables and d_1 as follows,

$$\begin{cases} \dot{z}_{21} = z_{22} + l_{21}\left(x_1 - z_{21}\right), \\ \dot{z}_{22} = Mz_{22} + Nz_{21} + g_q u_q + z_{13} + z_{23} + l_{22}\left(x_1 - z_{21}\right), \\ \dot{z}_{23} = l_{23}\left(x_1 - z_{21}\right), \end{cases} \tag{9}$$

where z_{21}, z_{22} and z_{23} are the estimations of x_1, x_2 and d_1. l_{21}, l_{22} and l_{23} are observer gains of the second ESO. After the second ESO, the estimation error of disturbance is as follows,

$$d_2 = x_3 - z_{13} - z_{23}. \tag{10}$$

And so on, after the $(n-1)$th ESO, the disturbance estimation error is $d_{n-1} = x_3 - z_{13} - z_{23} - ... - z_{(n-1)3}$.

Assumption 3. The derivative of $d_2, ..., d_{n-1}$ $(n \geq 2, n \in N^+)$ are bounded and define $\zeta_2 = \sup_{t>0} ||\dot{d}_2||, ..., \zeta_{n-1} = \sup_{t>0} ||\dot{d}_{n-1}||$.

Then the nth model-assisted ESO is designed as,

$$\begin{cases} \dot{z}_{n1} = z_{n2} + l_{n1}\left(x_1 - z_{n1}\right), \\ \dot{z}_{n2} = Mz_{n2} + Nz_{n1} + g_q u_q + z_{13} + z_{23} + ... + z_{n3} + l_{n2}\left(x_1 - z_{n1}\right), \\ \dot{z}_{n3} = l_{n3}\left(x_1 - z_{n1}\right), \end{cases} \tag{11}$$

where z_{n1}, z_{n2} and z_{n3} are the estimations of x_1, x_2 and d_{n-1}.

After the n-level model-assisted cascaded ESO, the estimated total disturbance is obtained as,

$$\hat{z}_n = z_{13} + z_{23} + ... + z_{n3}, \tag{12}$$

and the disturbance estimation error is

$$d_n = x_3 - \hat{z}_n. \tag{13}$$

Theorem 1. Consider the speed-current single-loop structure of PMSM (5) and its corresponding n-level model-assisted cascaded ESO (7), (9) and (11). Under the assumption 1, 2 and 3, by choosing the parameters of ith model-assisted ESO ($1 \leq i \leq n$, $i \in N^+$) as $l_{i1} = M + 3\alpha_i$, $l_{i2} = 3\alpha_i^2 + 3\alpha_i M + M^2 + N$ and $l_{i3} = \alpha_i^3 (\alpha_i > 0$ is the observer bandwidth of ith model-assisted ESO), the estimation errors e_i are bounded for any finite time $t > 0$. In addition, increasing the observer bandwidth α_i can reduce the estimation error and increase the convergence rate. What's more, if the lumped disturbance d_0 is slow time-varying, the n-level model-assisted cascaded ESO is asymptotically stable.

Proof. From (6), (7), (9) and (11), the n-level cascaded ESO observation error dynamic can be represented as

$$\dot{e}_i = A_i e_i + B\dot{d}_{i-1}, \tag{14}$$

where $e_i = x - z_i$, $z_i = \begin{bmatrix} z_{i1} \\ z_{i2} \\ z_{i3} \end{bmatrix}$, $A_i = \begin{bmatrix} -l_{i1} & 1 & 0 \\ -l_{i2}+N & M & 1 \\ -l_{i3} & 0 & 0 \end{bmatrix}$, $B = \begin{bmatrix} 0 \\ 0 \\ 1 \end{bmatrix}$. The characteristic polynomial of A_i can be expressed as follows

$$\lambda_i(s) = s^3 + \left(l_{i1} - M\right) s^2 + \left(l_{i2} - N - M l_{i1}\right) s + l_{i3}. \tag{15}$$

If the desired bandwidth of the ith ESO is chosen as $\alpha_i (\alpha_i > 0)$, which is the only tuning parameter to be adjusted and the implementation process much simplified, compared to other observers. Then (15) can also be expressed as

$$\lambda_i(s) = \left(s + \alpha_i\right)^3 = s^3 + 3\alpha_i s^2 + 3\alpha_i^2 s + \alpha_i^3, \tag{16}$$

and l_{i1}, l_{i2} and l_{i3} are determined as follows

$$\begin{cases} l_{i1} = M + 3\alpha_i, \\ l_{i2} = 3\alpha_i^2 + 3\alpha_i M + M^2 + N, \\ l_{i3} = \alpha_i^3. \end{cases} \tag{17}$$

Therefore, A_i is Hurwitz for $\alpha_i > 0$ with eigenvalues $\lambda_{ij} = -\alpha_i < 0$ $(j = 1, 2, 3)$ and the dynamic (14) is stable. It can obtain that[34],

$$\exp^{A_i t} = \sum_{j=1}^{3} W_j \left[\frac{t^{j-1}}{(j-1)!}\right] \exp^{-\alpha_i t}, \tag{18}$$

where $W_j \in \mathbb{R}^{3\times 3}$. So

$$||\exp^{A_i t}|| \leq \sum_{j=1}^{3} ||W_j|| \left[\frac{t^{j-1}}{(j-1)!}\right] \exp^{-\alpha_i t}. \tag{19}$$

Then, for every $\delta > 0$, such that $\rho_i = (\alpha_i - \delta) > 0$, there exists a constant P_i that satisfies

$$||\exp^{A_i t}|| \leq \sum_{j=1}^{3} ||W_j|| \left[\frac{t^{j-1}}{(j-1)!}\right] \exp^{-\alpha_i t} \leq P_i \exp^{-\rho_i t}. \tag{20}$$

Since $\zeta_{i-1} = \sup_{t>0} |\dot{d}_{i-1}|$, the estimation error in (14) satisfies

$$||e_i(t)|| \leq P_i \exp^{-\rho_i (t-t_0)} \left[||e(t_0)|| - \frac{\zeta_{i-1}}{\rho_i}\right] + \frac{P_i \zeta_{i-1}}{\rho_i}, t \geq t_0. \tag{21}$$

And

$$\lim_{t\to\infty} ||e_i(t)|| = \frac{P_i \zeta_{i-1}}{\rho_i}. \tag{22}$$

It means that the estimated state z_{ij} converge exponentially to a bounded ball around the system state x_i. In addition, it can be seen that increasing the ESO bandwidth α_i result in faster convergence rate and smaller ball radius of the estimation error. What's more, if $\dot{d}_0$ is slow time-varying as $\dot{d}_0 = 0$, then $\lim_{t\to\infty} e_i(t) = 0$, the n-level model-assisted cascaded ESO is asymptotically stable. This completes the proof.

3.2 | Frequency-domain analysis of model-assisted cascaded ESO

The transfer function from the total disturbance to disturbance estimation error in the frequency domain is analyzed to obtain the ability of the model-assisted cascaded ESO estimation of disturbance.

In the first ESO, the transfer function of the total disturbance d_0 to the estimated value z_{13} in (7) in the frequency domain is as follows,

$$\frac{Z_{13}(s)}{D_0(s)} = \frac{\alpha_1^3}{s^3 + 3\alpha_1 s^2 + 3\alpha_1^2 s + \alpha_1^3}. \tag{23}$$

So the transfer function of the total disturbance d_0 to the disturbance estimation error d_1 is as follows,

$$\begin{aligned} \frac{D_1(s)}{D_0(s)} &= \frac{D_0(s) - Z_{13}(s)}{D_0(s)} = 1 - \frac{Z_{13}(s)}{D_0(s)} \\ &= \frac{s^3 + 3\alpha_1 s^2 + 3\alpha_1^2 s}{s^3 + 3\alpha_1 s^2 + 3\alpha_1^2 s + \alpha_1^3} = \frac{s \times (s^2 + 3\alpha_1 s + 3\alpha_1^2)}{s^3 + 3\alpha_1 s^2 + 3\alpha_1^2 s + \alpha_1^3}. \end{aligned} \tag{24}$$

Based on (9), the estimation error transfer function of 2-level cascaded ESO is

$$\begin{aligned}&\frac{D_0(s)-Z_{13}(s)-Z_{23}(s)}{D_0(s)}=1-\frac{Z_{13}(s)+Z_{23}(s)}{D_0(s)}\\&=\frac{s^3+3\alpha_1 s^2+3\alpha_1^2 s}{s^3+3\alpha_1 s^2+3\alpha_1^2 s+\alpha_1^3}\times\frac{s^3+3\alpha_2 s^2+3\alpha_2^2 s}{s^3+3\alpha_2 s^2+3\alpha_2^2 s+\alpha_2^3}\\&=\frac{s^2\times(s^2+3\alpha_1 s+3\alpha_1^2)\times(s^2+3\alpha_2 s+3\alpha_2^2)}{(s^3+3\alpha_1 s^2+3\alpha_1^2 s+\alpha_1^3)\times(s^3+3\alpha_2 s^2+3\alpha_2^2 s+\alpha_2^3)}.\end{aligned}\tag{25}$$

So the estimation error transfer function of the n-level cascaded ESO is

$$\begin{aligned}&1-\frac{Z_{13}(s)+Z_{23}(s)+\ldots+Z_{n3}(s)}{D_0(s)}\\&=\frac{s^n\times(s^2+3\alpha_1 s+3\alpha_1^2)\times\ldots\times(s^2+3\alpha_n s+3\alpha_n^2)}{(s^3+3\alpha_1 s^2+3\alpha_1^2 s+\alpha_1^3)\times\ldots\times(s^3+3\alpha_n s^2+3\alpha_n^2 s+\alpha_n^3)}.\end{aligned}\tag{26}$$

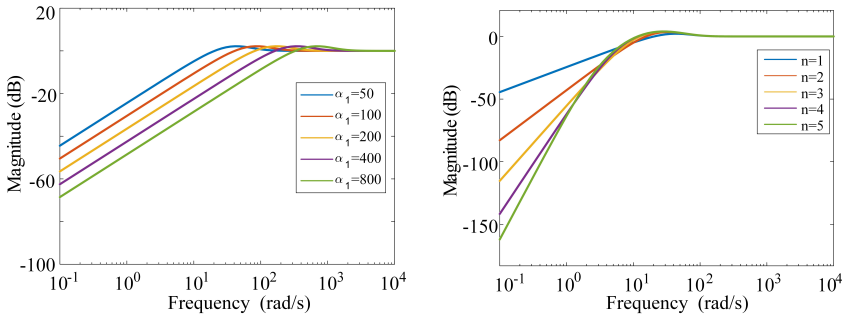

(a) Bode diagram of single ESO (b) Bode diagram of n-level cascaded ESO

Figure 3 Bode diagram of single ESO and n-level cascaded ESO

Fig. 3(a)-(b) show the Bode diagram of estimation error transfer function of single ESO and n-level cascaded ESO. In Fig. 3(a), the bandwidths of ESOs are $\alpha_1 = 50$, $\alpha_1 = 100$, $\alpha_1 = 200$, $\alpha_1 = 400$ and $\alpha_1 = 800$, respectively. In Fig. 3(b), n ranges from 1 to 5 and the bandwidths of n-level cascaded ESOs are $\alpha_1 = 50$, $\alpha_2 = \alpha_1/2$, $\alpha_3 = \alpha_1/2^2$, $\alpha_4 = \alpha_1/2^3$, $\alpha_5 = \alpha_1/2^4$, respectively. As can be seen from Fig. 3(a), with the increase of bandwidth, magnitude of transfer function decreases in the low frequency band. Evidently, the larger bandwidth leads to the more rapid speed to estimate the disturbance. As can be seen from Fig. 3(b), with the increase of n, the slope of the amplitude-frequency curve is larger in the low frequency band. The cascaded ESO can obtain a smaller amplitude than the single ESO, and thus a faster disturbance estimation without increasing bandwidth. Therefore, cascaded ESO is more accurately and quickly than single ESO of estimating disturbance without increasing bandwidth.

3.3 | Design of composite controller

In order to eliminate the residual disturbance d_n and reduce chatterings, a composite controller based on model-assisted cascaded ESO and SMC is designed.

The speed error of the PMSM is defined as $\Delta = \omega^* - \omega$, and the sliding mode surface is designed based on the disturbance error of the n-level model-assisted cascaded ESO of (13) as

$$S = \dot{\Delta} + c_1\Delta + d_n,\tag{27}$$

where $c_1 > 0$.

With the feedforward of estimation disturbance and the state $\hat{\omega}$ from the model-assisted cascaded ESO designed above, the controller is constructed. Then, the controller u_q is obtained as

$$\begin{aligned} u_q &= g_q^{-1}\left[\ddot{\omega}^* - M\hat{\dot{\omega}} - N\omega + c_1\dot{\Delta} - \hat{z}_n\right] - g_q^{-1}c_2 sgn(S) \\ &= g_q^{-1}\left[\ddot{\omega}^* + c_1\dot{\omega}^* - \left(M + c_1\right)\hat{\dot{\omega}} - N\omega - \hat{z}_n - c_2 sgn(S)\right], \end{aligned} \tag{28}$$

where

$$c_2 = \varepsilon_n + \zeta_n + \eta_n + k \tag{29}$$

is the switching gain, $\varepsilon_n = \sup_{t>0}||d_n||$, $\zeta_n = \sup_{t>0}||\dot{d}_n||$, $\eta_n = (M + c_1)\sup_{t>0}||e_{n2}|| = (M + c_1)\sup_{t>0}||\dot{\omega} - z_{n2}||$, $k > 0$.

The flowchart of the model-assisted cascaded ESO based SMC scheme for speed regulation is shown in Fig.4.

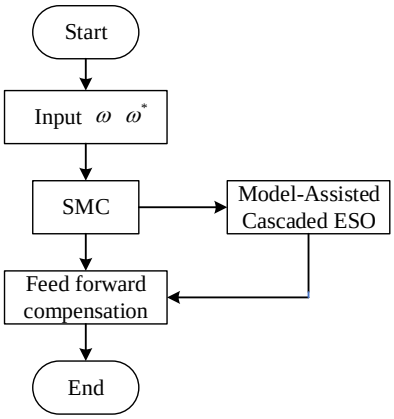

Figure 4 Flowchart of the model-assisted cascaded ESO based SMC scheme for speed regulation

Lemma 1. [35] For the system $\dot{x} = g(x)$, $x(0) = 0$, if there is a Lyapunov function $V(x)$ satisfying $\dot{V}(x) \leq -\alpha V^p(x)$, where $\alpha > 0$, $0 < p < 1$, then $x = 0$ is finite-time stable equilibrium of the system.

Theorem 2. For the PMSM system (5) with the proposed sliding-mode (27), if the controller is designed as (28) and the switching gain satisfies (29) based on the proposed cascaded ESO above, then the output tracking error converges to a neighborhood of the origin. What's more, if the lumped disturbance d_0 is slow time-varying, the closed loop system will asymptotically converge to the reference speed.

Proof. Based on (27) and (28), the time derivative of the sliding mode surface S is

$$\begin{aligned} \dot{S} &= \ddot{\Delta} + c_1\dot{\Delta} + \dot{d}_n \\ &= \ddot{\omega}^* - M\dot{\omega} - N\omega - g_q u_q - d_0 + c_1(\dot{\omega}^* - \dot{\omega}) + \dot{d}_n \\ &= -d_n + \dot{d}_n - (M + c_1)e_{n2} - c_2 sgn(S). \end{aligned} \tag{30}$$

A Lyapunov function is considered as

$$V = \frac{1}{2}S^2. \tag{31}$$

The time derivative of V is as follows,

$$\begin{aligned} \dot{V} &= S\dot{S} \\ &= -d_n S + \dot{d}_n S - (M + c_1)e_{n2}S - c_2||S|| \\ &\leq (||d_n|| + ||\dot{d}_n|| + (M + c_1)||e_{n2}|| - c_2)||S|| \\ &\leq (\varepsilon_n + \zeta_n + \eta_n - c_2)||S|| \\ &= -k||S|| \\ &= -\sqrt{2}kV^{\frac{1}{2}}. \end{aligned} \tag{32}$$

It is concluded that the state can reach the sliding surface in finite time from Lemma 1. In addition, (32) also ensures that the state will be limited to the surface $S = 0$ at all times in the future.

According to the definition of S in (27), when the state reach the sliding surface,

$$\dot{\Delta} = -c_1\Delta - d_n. \tag{33}$$

It can obtain that

$$\Delta = p\exp^{-c_1 t} - \frac{d_n}{c_1}, \tag{34}$$

where p is a constant. So

$$||\Delta|| \leq |p|\exp^{-c_1 t} + \frac{\varepsilon_n}{c_1}. \tag{35}$$

As t approaches infinity, there is $\lim_{t\to\infty} ||\Delta(t)|| = \frac{\varepsilon_n}{c_1}$. So the output tracking error converges to a neighborhood of the origin. What's more, if $\dot{d}_0$ is slow time-varying as $\dot{d}_0 = 0$, then $d_n = 0$, so $\lim_{t\to\infty} \Delta = 0$ and $\lim_{t\to\infty} \dot{\Delta} = 0$ can be concluded. Thus, the closed loop system will asymptotically converge to the reference speed. This completes the proof. □

4 | SIMULATIONS AND EXPERIMENTS

In this section, to evaluate the performance of this method, the influence of parameters, simulations, introduction of experimental control platform with three-level neutral-point-clamped (NPC) inverter and experiments are performed, respectively. The nominal specifications of the PMSM is shown in Table 1.

Table 1 The nominal specifications of the PMSM

Parameters	Label	Value
rated power	P_{rated}	730W
rated voltage	V_{rated}	220V
rated current	I_{rated}	3A
rated speed	ω_{rated}	2000rpm
rated torque	τ_{rated}	3.5N·m
pole pairs	n_p	4
inductance	L_0	4.85mH
stator resistance	R_{s0}	2.03Ω
inertia constant	J_{m0}	0.00034Kg · m^2
magnetic flux constant	Φ_0	0.13065Wb

4.1 | Influence of Parameters

The reference speed ω^* in simulations is set as 300rpm. PMSM starts with no load and the load torque is suddenly changed from 0 to 5N·m at $t = 0.5s$. The control variable method is applied in comparative simulations, and only one parameter will be changed[25]. The bandwidths of n-level cascaded ESO are $\alpha_1 = 40$, $\alpha_2 = \alpha_1/2$, ... , $\alpha_n = \alpha_1/2^{n-1}$ and $n = 2$, respectively. The parameters of the (28) are designed as follows: $c_1 = 800000$, $c_2 = 200000$. The parameters of PI controller in d-axis current are $k_{cp} = 12.75$ and $k_{ci} = 5338.55$. To evaluate the control results qualitatively, the performance specification including overshoot (OS), settling time (ST), recovery time(RT), speed fluctuation(SF) at the phase of loading, root-mean-square error of q-axis current(RQ) are utilized for validation.

4.1.1 | Effect of n

Fig.5(a)-(b) are the comparison curves of speed and i_q from $n = 1$ to $n = 3$, respectively. In the case of $n = 1$, it is the single-loop composite controller of SMC and ESO (SLSMC+ESO).The performance indices are tabulated in Table 2. The larger n is, the quicker settling time, smaller speed fluctuation and smaller i_q chattering are. However, overshoot occurs at the startup in the case of $n = 3$. There is no speed overshoot but some speed chatterings at the phase of power-on in the case of $n = 1$ and $n = 2$. Because linear observer tends to produce overshoot output when the observed signal has a step change[36], too much n can cause overshoot easily. Therefore, in order to achieve good control performance, $n = 2$ is selected in the proposed algorithm.

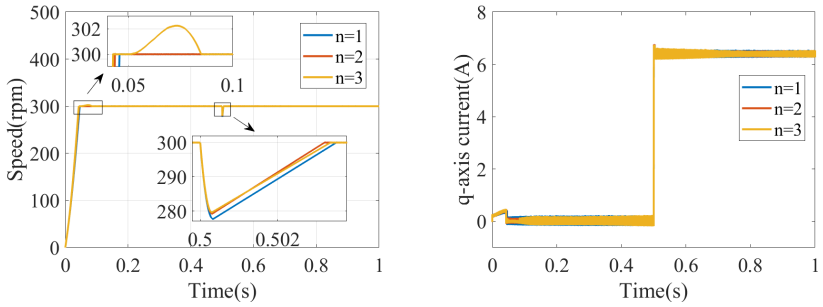

(a) speed responses (b) i_q responses

Figure 5 comparison curves of different n

Table 2 Performance indices in the simulation of different n

Performance	OS(rpm)	ST(s)	RT(s)	SF(rpm)	RQ(A)
$n = 1$	0	0.046	0.0035	22.303	0.1263
$n = 2$	0	0.044	0.0032	20.754	0.1175
$n = 3$	2.26	0.043	0.0033	20.347	0.1163

4.1.2 | Effect of c_1

Fig. 6(a)-(b) are the comparison curves of speed and i_q from $c_1 = 400000$ to $c_1 = 1000000$, respectively. The performance indices are tabulated in Table 3. The smaller c_1 is, the quicker settling time and recovery time and smaller speed fluctuation are, but too small c_1 causes chatterings and overcurrent in q-axis.

Remark 1. Choosing a suitable c_1 can balance fast dynamic performance and q-axis current constraint.

4.1.3 | Effect of c_2

Fig. 7(a)-(b) are the comparison curves of speed and i_q from $c_2 = 300000$ to $c_2 = 100000$, respectively. The performance indices are tabulated in Table 4. The larger c_2 is, the quicker settling time and recovery time and smaller speed fluctuation are, but the i_q chattering increased.

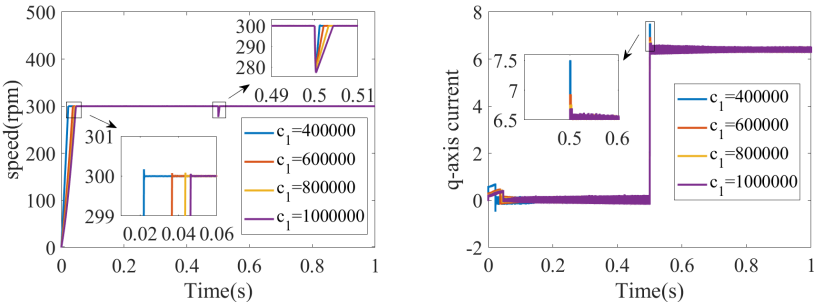

(a) speed responses (b) i_q responses

Figure 6 comparison curves of different c_1

Table 3 Performance indices in the simulation of different c_1

Performance	ST(s)	RT(s)	SF(rpm)	RQ(A)
$c_1 = 400000$	0.022	0.0012	19.785	0.3126
$c_1 = 600000$	0.036	0.0021	20.071	0.1137
$c_1 = 800000$	0.044	0.0032	20.754	0.1175
$c_1 = 1000000$	0.047	0.0043	22.712	0.1230

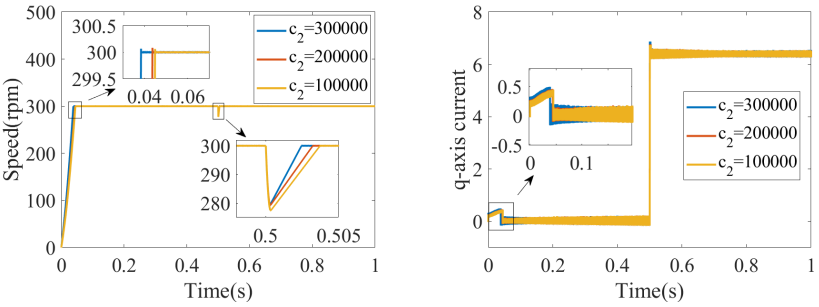

(a) speed responses (b) i_q responses

Figure 7 comparison curves of different c_2

Table 4 Performance indices in the simulation of different c_2

Performance	ST(s)	RT(s)	SF(rpm)	RQ(A)
$c_2 = 100000$	0.045	0.0037	22.597	0.1068
$c_2 = 200000$	0.044	0.0032	20.754	0.1175
$c_2 = 300000$	0.038	0.0025	20.519	0.1211

4.2 | Simulations

There are four groups of simulations. The first one is acceleration after the PMSM is powered on, the second one is sudden loading and the last is internal parameter perturbations, respectively. It can be verified that the proposed method has good robust while maintaining good dynamic and static performance. The proposed method controller is compared with conventional

double-loop SMC controller (DLSMC) and SLSMC+ESO. The DLSMC can be expressed as[25]

$$i_q^* = \frac{2J_m}{3n_p\Phi}\int_0^t[\lambda(-\dot{\omega}) + \eta\text{sgn}(\lambda(\omega^* - \omega) - \dot{\omega})]. \tag{36}$$

To guarantee relatively fair, the control parameters of controllers are chosen to be relatively optimal after many repeated tests such that take into account dynamic and static performance such as overshoot, settling time, recovery time, robust, current constraint and so on. The control parameters of the simulations are presented in Table 5. The parameters of PI in current loop in surface-mounted PMSM can be designed as $k_{cp} = \alpha L$ and $k_{ci} = \alpha R_s$, where $\alpha = 2\pi/\tau$ is the bandwidth of current loop bandwidth and $\tau = L/R_s$ is the time constant of the PMSM[25]. Therefore, the parameters of PI controller in d-axis current, coordinated by these three comparison methods, are $k_{cp} = 12.75$ and $k_{ci} = 5338.55$.

Table 5 Control parameters in simulations

Control algorithm	Parameter and Value
DLSMC	$\lambda = 800$, $\eta = 60000000$
SLSMC+ESO	$c_1 = 200000$, $c_2 = 40000$, $\alpha_1 = 100$
the proposed method	$c_1 = 200000$, $c_2 = 40000$, $\alpha_1 = 100$, $\alpha_2 = 10$

4.2.1 | phase of acceleration

The process of simulation is the reference speed is 300rpm at startup and 1000rpm after 0.2s. The comparison speed and i_q curves under different controllers when acceleration are shown in Fig.8. To evaluate the control results qualitatively, the performance specification including settling time(ST), root-mean-square steady-state error of q-axis current(RSQ) are utilized for validation. The performance indices are tabulated in Table 6.

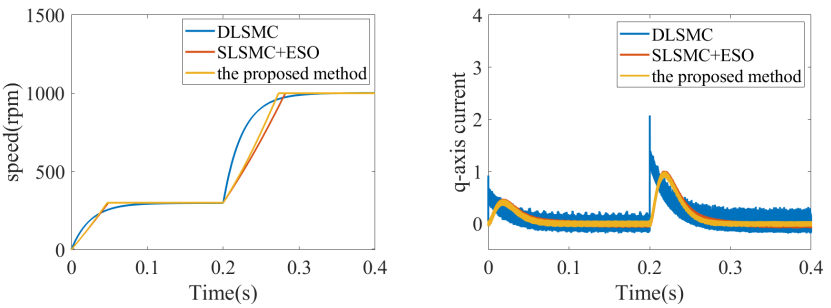

(a) speed responses (b) i_q responses

Figure 8 comparison curves at the phase of acceleration under DLSMC, SLSMC+ESO and the proposed method

Table 6 Performance indices in the acceleration simulation of different controllers

Performance	ST(s)	RSQ(A)
DLSMC	0.106	0.0985
SLSMC+ESO	0.083	0.0247
the proposed method	0.071	0.0234

As shown in Fig.8 and Table 6, the PMSM can reach the reference speed faster under the proposed method than SLSMC+ESO and DLSMC. What's more, the chatterings of i_q under the proposed method are smaller than that of SLSMC+ESO and DLSMC. Therefore, the proposed method has the advantages of fast dynamic performance and small chatterings.

4.2.2 | phase of a sudden load torque disturbance

The process of simulation is adding a sudden load torque of 5N·m when PMSM is running at the speed of 800rpm. The comparison curves under different controllers are shown in Fig.9. To evaluate the control results qualitatively, the performance specification including recovery time(RT), speed fluctuation(SF) when loading, root-mean-square steady-state error of q-axis current(RSQ) are utilized for validation. The performance indices are tabulated in Table 7.

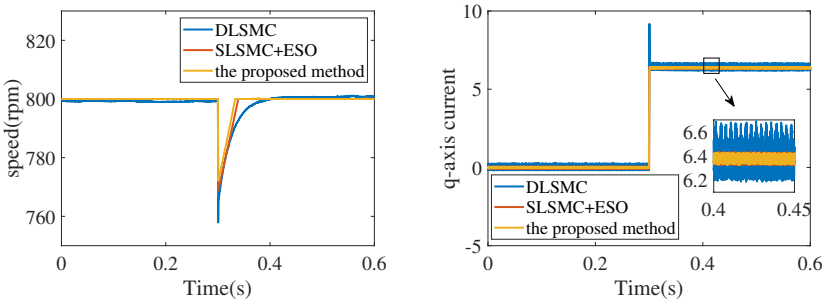

(a) speed responses (b) i_q responses

Figure 9 comparison curves at the phase of sudden loading under DLSMC, SLSMC+ESO and the proposed method

Table 7 Performance indices in the loading simulation of different controllers

Performance	RT(s)	SF(rpm)	RSQ(A)
DLSMC	0.0942	42.098	0.0945
SLSMC+ESO	0.0387	31.136	0.0268
the proposed method	0.0330	27.853	0.0221

As shown in Fig. 9 and Table 7, when loading, there is smaller speed fluctuation and less recovery time under the proposed method than SLSMC+ESO and DLSMC. Similarly, the chatterings of i_q under the proposed method are smaller than those of SLSMC+ESO and DLSMC. Therefore, the proposed method has the advantages of good robust and small chatterings.

4.2.3 | phase of parameter perturbations

The simulation process is that the stator resistance R_s or stator inductance L have parameter perturbations during the operation of the PMSM.

The actual R_s parameter is randomly changed $\pm 50\%$ on the basis of its nominal value at 2000rpm. The comparison curves under different controllers are shown in Fig.10. To evaluate the control results qualitatively, the performance specification including root-mean-square steady-state error of speed(RSS) and root-mean-square steady-state error of q-axis current (RSQ) are

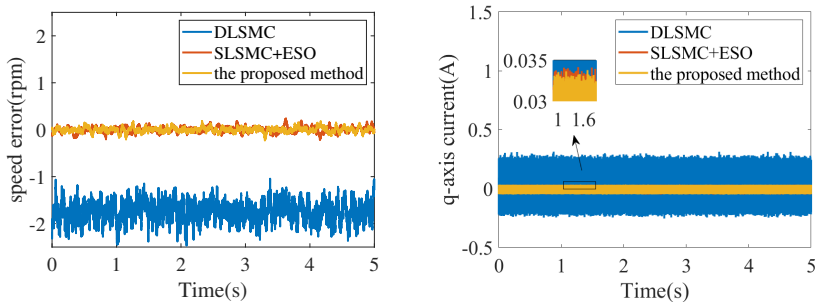

(a) speed responses (b) q-axis current responses

Figure 10 comparison curves at the phase of R_s perturbations under DLSMC, SLSMC+ESO and the proposed method

Table 8 Performance indices in the R_s perturbations simulation of different controllers

Performance	RSS(rpm)	RSQ(A)
DLSMC	1.7511	0.0935
SLSMC+ESO	0.0725	0.0137
the proposed method	0.0537	0.0135

utilized for validation. The performance indices are tabulated in Table 8. As shown in Fig.10 and Table 8, there is smaller root-mean-square steady-state error of speed and q-axis current under the proposed method than SLSMC+ESO and DLSMC with R_s perturbations. Therefore, the proposed method has the advantages of good robust and small chatterings.

The actual L parameter is randomly changed $\pm 25\%$ on the basis of its nominal value at 2000rpm. The comparison curves under different controllers are shown in Fig.11. To evaluate the control results qualitatively, the performance specification including RSS and RSQ are utilized for validation. The performance indices are tabulated in Table 9. As shown in Fig.11 and Table 9 , there is smaller chatterings, root-mean-square steady-state error of speed and q-axis current under the proposed method than SLSMC+ESO and DLSMC with L perturbations. Therefore, the proposed method has the advantages of good robust and small chatterings.

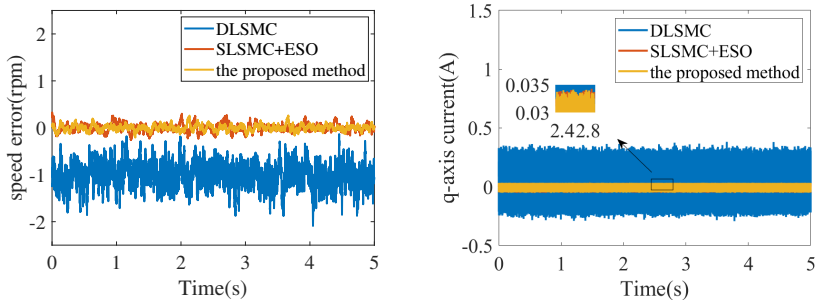

(a) speed responses (b) q-axis current responses

Figure 11 comparison curves at the phase of L perturbations under DLSMC, SLSMC+ESO and the proposed method

Table 9 Performance indices in the L perturbations simulation of different controllers

Performance	RSS(rpm)	RSQ(A)
DLSMC	1.0034	0.0862
SLSMC+ESO	0.0822	0.0136
the proposed method	0.0617	0.0135

4.3 | The experimental control platform with three-level NPC inverter

The experimental control platform is built to drive a 730W PMSM. The DC bus voltage is 220V. The controller adopts TMS320F28335 and the PMSM is driven by a three-level NPC inverter. To test the load disturbance of the proposed method under different conditions, the external load is given by another PMSM with the same power. The experimental platform is shown in Fig.12.

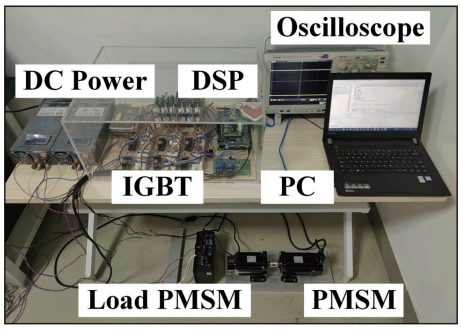

Figure 12 Photo of the experimental platform

Three-level NPC inverter has the advantages of low output current harmonic content, low voltage of a single switching device, and the output PWM waveform is closer to sine wave than the conventional two-level NPC inverter, suitable for high voltage and high power industrial control field. In the application of PMSM drive system, the use of three-level NPC inverter can have better power quality than the conventional two-level NPC inverter[8]. The topology of three-level NPC inverter in this paper is shown in Fig. 13.

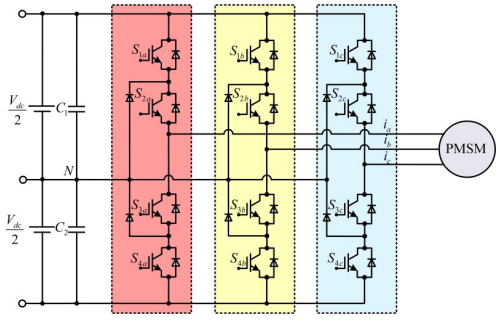

Figure 13 Three-level NPC topology

Compared with the two-level NPC inverter structure, the three-level NPC topology has four IGBTs in a single bridge arm, and its control method is relatively complex. As shown in Fig. 14, the three-level NPC inverter has 27 voltage vectors. There are 8 redundant voltage vectors and 18 non-redundant voltage vectors. There are three zero vectors of three-level NPC inverter,

namely PPP, NNN and OOO, and twelve small vectors, namely POO, ONN, PPO, OON, OPO, NON, OPP, NOO, OOP, NNO, POP, ONO, and 6 medium vectors, namely PON, OPN, NPO, NOP, ONP and PNO, and six large vectors, namely PNN, PPN, NPN, NPP, NNP and PNP.

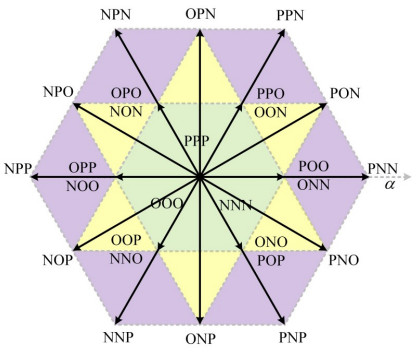

Figure 14 Voltage vectors of three-level NPC inverter

4.4 | Experiments

There are four groups of experiments. The first one is acceleration, the second one deceleration, the third one is sudden loading and the last one is parameter perturbations, respectively. The experimental results show that the controller has fast dynamic performance, small chatterings and good robustness.

To guarantee relatively fair, the control parameters of controllers are chosen to be relatively optimal after many repeated tests such that take into account dynamic and static performance such as overshoot, settling time, recovery time, robust, current constraint and so on. The control parameters of the experiments are presented in Table 10. The parameters of PI controller in d-axis current, coordinated by these three comparison methods, are $k_{cp} = 0.1$ and $k_{ci} = 0.6$.

Table 10 Control parameters in experiments

Control algorithm	Parameter and Value
DLSMC	$\lambda = 200, \eta = 1000000$
SLSMC+ESO	$c_1 = 400000, c_2 = 30000, \alpha_1 = 90$
the proposed method	$c_1 = 400000, c_2 = 30000, \alpha_1 = 90, \alpha_2 = 10$

4.4.1 | Phase of acceleration

There are two experiments of acceleration. The speed of the first one is 200rpm to 800rpm, the second one is 1500rpm to 2000rpm. Fig. 15(a)-(c) and Fig. 16(a)-(c) are speed, i_d and i_q response curves under different controllers of two experiments. Corresponding speed regulation performance indices, including ST, root-mean-square steady-state error of speed(RSS), root-mean-square steady-state error of q-axis current(RSQ) and root-mean-square steady-state error of d-axis current(RSD) are utilized and shown in Table 11 and Table 12. It can be seen that there is no overshoot under the present method and SLSMC+ESO method, but there is obvious overshoot under the DLSMC method. Moreover, the proposed method has a faster tracking performance than SLSMC+ESO and DLSMC. What's more, the chatterings of speed, i_d and i_q under the control of the proposed method are smaller than those of SLSMC+ESO and DLSMC.

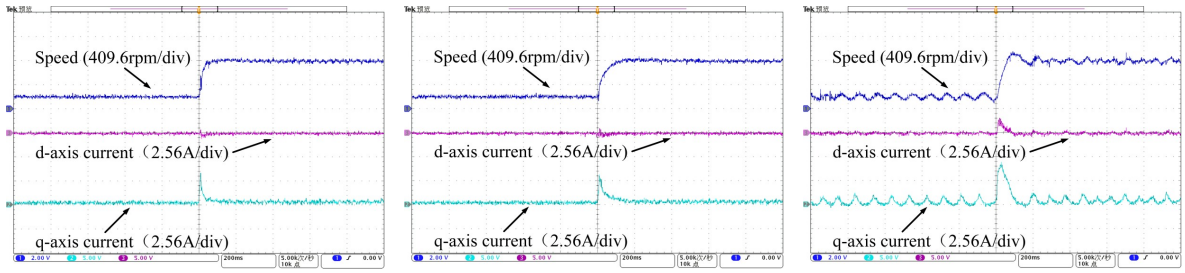

(a) Curves under the proposed method (b) Curves under SLSMC+ESO (c) Curves under DLSMC

Figure 15 Performance comparisons of acceleration under the prop sed method, SLSMC+ESO and DLSMC(200rpm-800rpm)

Table 11 Performance indices in the acceleration experiment(200rpm-800rpm) of different controllers

Performance	OT(rpm)	ST(ms)	RSS(rpm)	RSQ(A)	RSD(A)
DLSMC	80	150	33.04	0.54	0.13
SLSMC+ESO	0	130	24.38	0.34	0.12
the proposed method	0	75	22.26	0.33	0.11

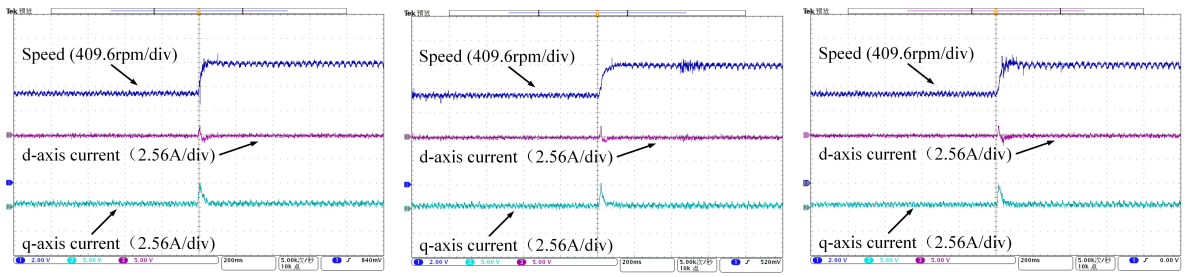

(a) Curves under the proposed method (b) Curves under SLSMC+ESO (c) Curves under DLSMC

Figure 16 Performance comparisons of acceleration under the proposed method, SLSMC+ESO and DLSMC(1500rpm-2000rpm)

Table 12 Performance indices in the acceleration experiment(1500rpm-2000rpm) of different controllers

Performance	OT(rpm)	ST(ms)	RSS(rpm)	RSQ(A)	RSD(A)
DLSMC	40	120	34.81	0.4075	0.14
SLSMC+ESO	0	100	28.54	0.35	0.13
the proposed method	0	60	26.37	0.34	0.12

4.4.2 | Phase of deceleration

There are two experiments of deceleration. The speed of the first one is 800rpm to 200rpm, the second one is 2000rpm to 1500rpm. Fig. 17(a)-(c) and Fig. 18(a)-(c) are speed, i_d and i_q response curves under different controllers of two experiments. Corresponding speed regulation performance indices, including OT, ST, RSS, RSQ and RSD are utilized and shown in Table 13 and Table 14. It can be seen that there is no excess speed overshoot under the proposed method compared to SLSMC+ESO and both the speed overshoot are smaller than that under DLSMC. What's more, the proposed method has a faster tracking

performance than SLSMC+ESO and DLSMC. Moreover, the chatterings of speed, i_d and i_q under the control of the proposed method are smaller than that of SLSMC+ESO and DLSMC.

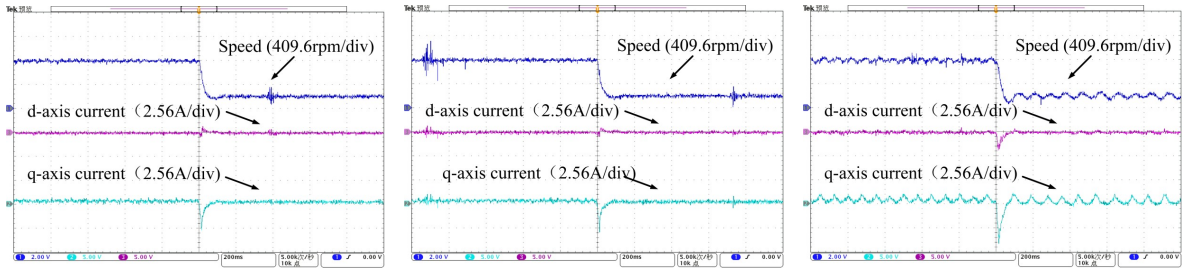

(a) Curves under the proposed method (b) Curves under SLSMC+ESO (c) Curves under DLSMC

Figure 17 Performance comparisons of deceleration under the proposed method, SLSMC+ESO and DLSMC(800rpm-200rpm)

Table 13 Performance indices in the deceleration experiment(800rpm-200rpm) of different controllers

Performance	OT(rpm)	ST(ms)	RSS(rpm)	RSQ(A)	RSD(A)
DLSMC	100	100	29.15	0.40	0.12
SLSMC+ESO	25	65	23.77	0.23	0.11
the proposed method	25	40	21.34	0.20	0.11

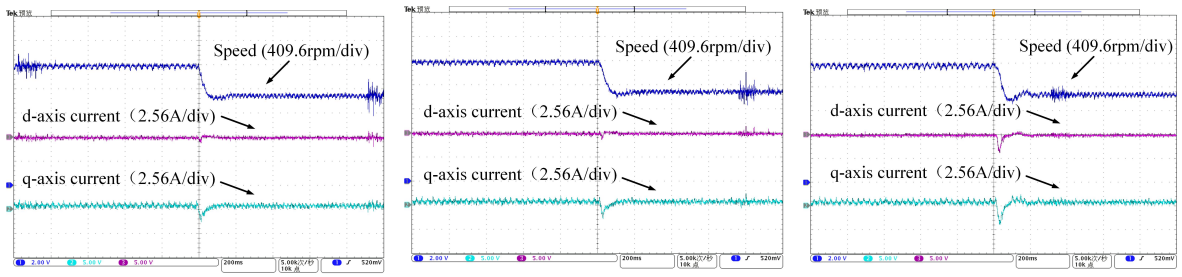

(a) Curves under the proposed method (b) Curves under SLSMC+ESO (c) Curves under DLSMC

Figure 18 Performance comparisons of deceleration under the proposed method, SLSMC+ESO and DLSMC(2000rpm-1500rpm)

4.4.3 | phase of a sudden load torque disturbance

The process of simulations are adding a sudden load torque $\tau_L = 1.2\text{N}\cdot\text{m}$ disturbance when PMSM is running at the speed of 800rpm, 1600rpm and 2000rpm, respectively. Fig. 19(a)-(c), Fig. 20(a)-(c) and Fig. 21(a)-(c) are speed, i_d, i_q response curves under different controllers of speed 800rpm, 1600rpm and 2000rpm, respectively. Corresponding speed regulation performance indices, including RT, SF, RSS, RSQ and RSD are utilized and shown in Table 15, Table 16 and Table 17. It can be seen that there are smaller speed fluctuations and less recovery time under the proposed method than SLSMC+ESO and DLSMC when loading. Similarly, the chatterings of i_q and i_d under the proposed method are smaller than those of SLSMC+ESO and DLSMC.

Table 14 Performance indices in the deceleration experiment(2000rpm-1500rpm) of different controllers

Performance	OT(rpm)	ST(ms)	RSS(rpm)	RSQ(A)	RSD(A)
DLSMC	100	120	32.5210	0.3379	0.1232
SLSMC+ESO	20	80	29.20	0.32	0.11
the proposed method	20	50	28.15	0.31	0.11

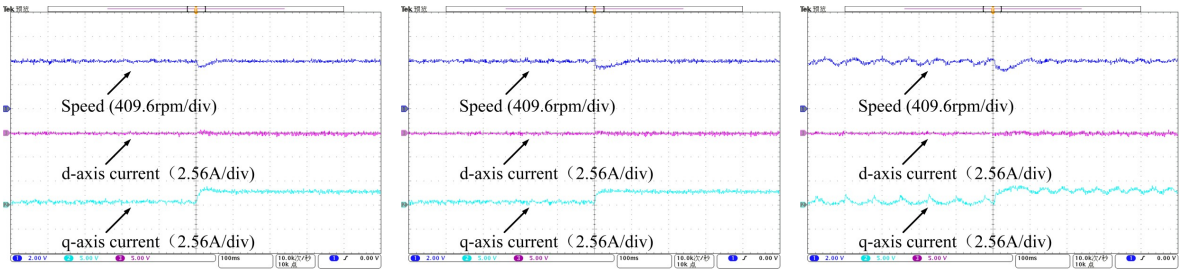

(a) Curves under the proposed method (b) Curves under SLSMC+ESO (c) Curves under DLSMC

Figure 19 Performance comparisons of a sudden load torque disturbance at the speed of 800rpm under the proposed method, SLSMC+ESO and DLSMC

Table 15 Performance indices in the loading experiment of 800rpm of different controllers

Performance	RT(ms)	SF(rpm)	RSS(rpm)	RSQ(A)	RSD(A)
DLSMC	85	180	37.21	0.72	0.20
SLSMC+ESO	80	155	29.00	0.18	0.17
the proposed method	56	105	27.70	0.13	0.15

Table 16 Performance indices in the loading experiment of 1600rpm of different controllers

Performance	RT(ms)	SF(rpm)	RSS(rpm)	RSQ(A)	RSD(A)
DLSMC	90	190	52.12	0.72	0.20
SLSMC+ESO	90	175	32.99	0.14	0.13
the proposed method	40	120	32.97	0.12	0.12

Table 17 Performance indices in the loading experiment of 2000rpm of different controllers

Performance	RT(ms)	SF(rpm)	RSS(rpm)	RSQ(A)	RSD(A)
DLSMC	100	240	33.81	0.69	0.13
SLSMC+ESO	90	180	28.35	0.13	0.12
the proposed method	50	130	26.66	0.12	0.11

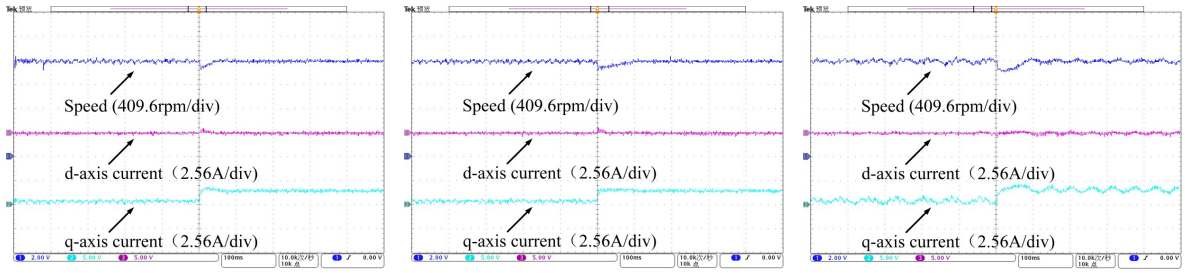

(a) Curves under the proposed method (b) Curves under SLSMC+ESO (c) Curves under DLSMC

Figure 20 Performance comparisons of a sudden load torque disturbance at the speed of 1600rpm under the proposed method, SLSMC+ESO and DLSMC

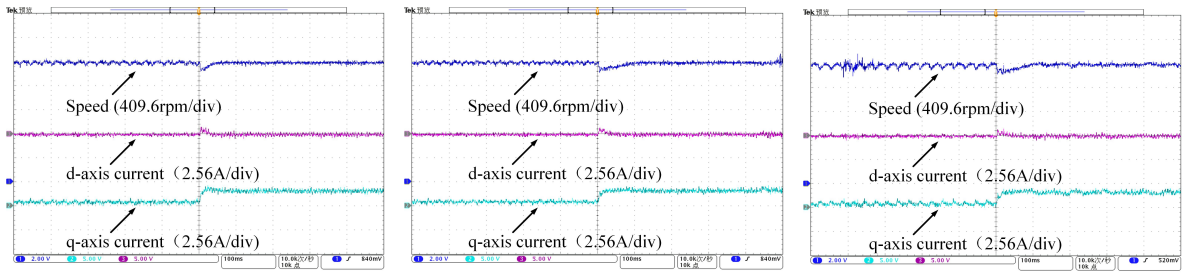

(a) Curves under the proposed method (b) Curves under SLSMC+ESO (c) Curves under DLSMC

Figure 21 Performance comparisons of a sudden load torque disturbance at the speed of 2000rpm under the proposed method, SLSMC+ESO and DLSMC

4.4.4 | phase of parameter perturbations

The stator resistance may increase due to the PMSM running temperature increase[37].The stator resistance R_s is changed by connecting the resistance 1Ω at the three-phase connection. The inductance parameter L can be changed by altering the value of the inductance parameter at the code composer studio (CCS) running interface. In the experiments, after long operation of PMSM, there is perturbation in the parameters such as inertia constant J_m, magnetic flux constant Φ and viscous friction coefficient B(let the nominal viscous friction coefficient $B_0 = 0$).

The inductance of the stator is increased by 1Ω. Fig. 22(a)-(c) are speed, i_d and i_q response curves under different controllers when the reference speed is 1000rmp. Corresponding speed regulation performance indices, including RSS, RSQ and RSD are utilized and shown in Table 18. It can be seen that the chatterings of speed, i_d and i_q under the control of the proposed method are smaller than those of SLSMC+ESO and DLSMC.

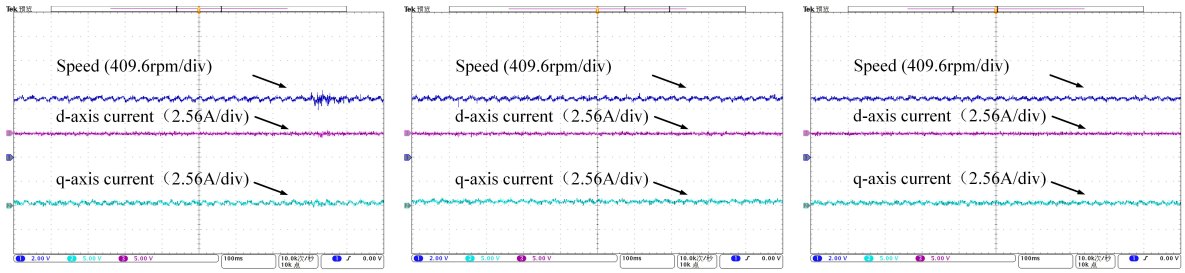

(a) Curves under the proposed method (b) Curves under SLSMC+ESO (c) Curves under DLSMC

Figure 22 Performance comparisons of R_s perturbations under the proposed method, SLSMC+ESO and DLSMC

Table 18 Performance indices in the R_s perturbations experiment of different controllers

Performance	RSS(rpm)	RSQ(A)	RSD(A)
DLSMC	30.1654	0.3332	0.1228
SLSMC+ESO	28.4674	0.3228	0.1199
the proposed method	25.3857	0.3122	0.1178

The parameter L in the algorithm is $L = 1.25L_0$. Fig. 23(a)-(c) are speed, i_d and i_q response curves under different controllers when the reference speed is 1000rmp. Corresponding speed regulation performance indices, including RSS, RSQ and RSD are utilized and shown in Table 19. It can be seen that the chatterings of speed, i_d and i_q under the control of the proposed method are smaller than those of SLSMC+ESO and DLSMC.

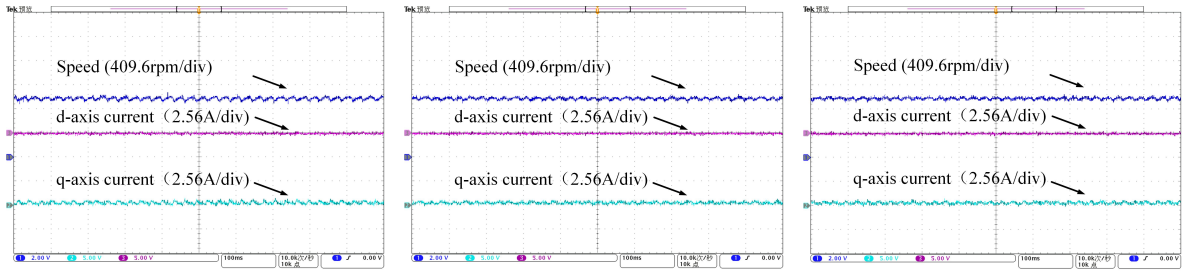

(a) Curves under the proposed method (b) Curves under SLSMC+ESO (c) Curves under DLSMC

Figure 23 Performance comparisons of L perturbations under the proposed method, SLSMC+ESO and DLSMC

Table 19 Performance indices in the L perturbations experiment of different controllers

Performance	RSS(rpm)	RSQ(A)	RSD(A)
DLSMC	35.1579	0.3172	0.1219
SLSMC+ESO	29.2841	0.3079	0.1215
the proposed method	23.5072	0.3039	0.1154

5 | CONCLUSIONS

In this paper, a novel speed-current single-loop controller based on model-assisted cascaded extended state observer (ESO) and sliding mode control (SMC) for the PMSM has been proposed. A model-assisted cascaded ESO based on model information is designed to estimate matched disturbance and unmatched disturbance for the second-order model of single-loop control of PMSM. This innovative approach not only allows for quick and accurate estimation of lump disturbance without increasing bandwidth, but also reduces the burden of ESO with model-assisted information. The controller has simple control structure, fast dynamic performance, small chatterings and good robustness. The simulation and experimental results on the PMSM have verified the effectiveness and robustness of the controller.

References

1. Adigintla S, Aware MV. Design and analysis of a speed controller for fractional-order-modeled voltage-source-inverter-fed induction motor drive. *Int J Circ Theor Appl*. 2022; 50(7): 2378-2397.

2. Yu F, Zhou C, Wang Z. Evaluation of model-free pemphictive current control in three-phase permanent magnet synchronous motor drives fed by three-level neutral-point-clamped inverters. *Int J Circ Theor Appl*. 2022; 50(11): 3968-3985.

3. Zhong L, Hu S. 60°phase difference current control-based open-phase fault-tolerant operation strategy for open-end winding permanent synchronous motor. *Int J Circ Theor Appl*. 2022; 50(10): 3409-3425.

4. Wang W, Liu C, Liu S, Song Z, Zhao H and Dai B. Current harmonic suppression for permanent-magnet synchronous motor based on Chebyshev filter and PI controller. *IEEE Trans. Magn.* 2021; 57(2): 1-6.

5. Wang C and Zhu Z Q. Fuzzy logic speed control of permanent magnet synchronous machine and feedback voltage ripple emphuction in flux-weakening operation region. *IEEE Trans. Ind. Appl.* 2020; 56(2): 1505-1517.

6. Xia C, Guo C and Shi T. A neural-network-identifier and fuzzy-controller-based algorithm for dynamic decoupling control of permanent-magnet spherical motor. *IEEE Trans. Ind. Electron.* 2010; 57(8): 2868-2878.

7. P Liu, Y Cui, C Wang, Y Liang, Z Chang, K Han, S Shen and G Zuo. Sensorless model predictive control based on I-f integrated sliding mode observer for surface permanent magnet synchronous motor. *Int J Circ Theor Appl*. 2023; 1-20.

8. Wang Q, Yu H, Li C, Lang X, Yeoh S, Yang T, Rivera M, Bozhko S and Wheeler P. A low-complexity optimal switching time-modulated model-predictive control for PMSM with three-level NPC converter. *IEEE Trans. Transp. Electr.* 2020; 6(3): 1188-1198.

9. Zhu L H, Zhang G Q, Jing R, Bi G D, Xiang R H, Wang G L and Xu D G. Nonlinear active disturbance rejection control strategy for permanent magnet synchronous motor drives. *IEEE Trans. on Energy Conver*. 2022; 37(3): 2119-2129.

10. Yin Z, Gong L, Du C, Liu J, Zhong Y. Integrated position and speed loops under sliding-mode control optimized by differential evolution algorithm for PMSM drives. *IEEE Trans. Power Electron.* 2019; 34(9): 8994-9005.

11. J Song, W Song, H Lin. DC-link voltage control of small capacitor PMSM drive system based on MPC algorithm. *Int J Circ Theor Appl.* 2023; 1-18.

12. Z Wu, D Li, Y Liu, Y Chen. Performance analysis of improved ADRCs for a class of high-order processes with verification on main steam pressure control. *IEEE Trans. Ind. Electron.* 2023, 70(6): 6180-6190.

13. V Yousuf, A Ahmad. Optimal design and application of fuzzy logic equipped control in STATCOM to abate SSR oscillations. *Int J Circ Theor Appl.* 2021; 49(12): 4070-4087.

14. J Li, A Wu. Digital current-limited sliding-mode control for synchronous buck converter with curved switching surface. *Int J Circ Theor Appl.* 2021; 49: 536–553.

15. SK S, P S, K MS. An improved robust coupled sliding mode control strategy for solar photovoltaic-based single-phase inverters. *Int J Circ Theor Appl.* 2023; 51(5): 2163-2185.

16. Han J. From PID to active disturbance rejection control. *IEEE Trans. Ind. Electron.* 2009; 56(3):900–906.

17. Chen S and Chen Z. On active disturbance rejection control for a class of uncertain systems with measurement uncertainty. *IEEE Trans. Ind. Electron.* 2021; 68(2):1475–1485.

18. Xu W, Junejo A K, Liu Y and Islam M R. Improved continuous fast terminal sliding mode control with extended state observer for speed regulation of PMSM drive system. *IEEE Trans. Veh. Technol.* 2019; 68(11):10465-10476.

19. Qu L, Qiao W and Qu L. An extended-state-observer-based sliding-mode speed control for permanent-magnet synchronous motors. *IEEE J. Em. Sel. Top. P.* 2021; 9(2): 1605-1613.

20. Wang Y, Feng Y, Zhang X and Liang J. A new reaching law for antidisturbance sliding-mode control of PMSM speed regulation system. *IEEE Trans. Power Electron.* 2020; 35(4): 4117-4126.

21. Ma Y, Li D, Li Y and Yang L. A novel discrete compound integral terminal sliding mode control with disturbance compensation for PMSM speed system. *IEEE-ASME Trans. Mech.* 2022; 27(1): 549-560.

22. Tarczewski T and Grzesiak L. Constrained state feedback speed control of PMSM based on model pemphictive approach. *IEEE Trans. Ind. Electron.* 2016; 63(6): 3867-3875.

23. Hu Z and Hameyer K. A method of constraint handling for speedcontrolled induction machines. *IEEE Trans. Ind. Electron.* 2016; 63(7): 4061-4072.

24. Dai C, Guo T, Yang J and Li S H. A disturbance observer-based current-constrained controller for speed regulation of PMSM systems subject to unmatched disturbances. *IEEE Trans. Ind. Electron.* 2021; 68(1): 767-775.

25. Wang Y, Yu H and Liu L Y. Speed-current single-loop control with overcurrent protection for PMSM based on time-varying nonlinear disturbance observer. *IEEE Trans. Ind. Electron.* 2021; 69: 179-189.

26. Sun Z, Li S, Wang J, Zhang X and Mo X. Adaptive composite control method of permanent magnet synchronous motor systems. *Trans. Inst. Meas. Control*. 2018; 40(11): 3345-3357.

27. Rauf A, Yang J, Madonski R, Li S, and Wang Z. Sliding mode control of converter-fed DC motor with mismatched load torque compensation. *in Proc. 28th IEEE Int. Symp. Ind. Electronics*, 2019; 653-657.

28. Wang Y, Yu H, Feng N J and Wang C Y. Non-cascade backstepping sliding mode control with three-order extended state observer for pmsm drive. *IET Power Electron*. 2019; 13(6): 307-316.

29. Jiang W, Zhang L. Output-feedback sliding mode control for permanent magnet synchronous motor servo system subject to unmatched disturbances. *Math. Probl. Eng.* 2021; 2021: 1-11.

30. Khalil H K and Praly L. High-gain observers in nonlinear feedback control. *Int. J. Robust Nonlinear Control*. 2014; 24(6): 993-1015.

31. Łakomy K and Madonski R. Cascade extended state observer for active disturbance rejection control applications under measurement noise. *ISA Trans*. 2020; 109: 1-10.

32. Sun L, Li D, Gao Z, Yang Z and Zhao S. Combined feedforward and model-assisted active disturbance rejection control for non-minimum phase system. *ISA Trans*. 2016; 64: 24-33.

33. Patelski P, Dutkiewicz P. On the stability of ADRC for manipulators with modelling uncertainties. *ISA Trans*. 2020; 102: 295-303.

34. Lohmiller W and Slotine J J E. On contraction analysis for non-linear systems. *Automatica*. 1998; 34(6): 683-696.

35. Bhat S P and Bernstein D S. Finite-Time Stability of Continuous Autonomous Systems. *SIMA J. Contr. Opti.* 2000; 38(3):751-766.

36. Cunha J, Costa R R, Lizarralde F and Liu H. Peaking free variable structure control of uncertain linear systems based on a high-gain observer. *Automatica*. 2009; 45(5): 1156-1164.

37. Sul Seung-Ki.*Control of Electric Machine Drive Systems*. IEEE Press series on power engineering. 2011.ISBN 978-0-470-59079-9.